FEMS Yeast Research, 2025, **25**, foaf011
DOI: 10.1093/femsyr/foaf011
Advance access publication date: 13 March 2025
Research Article – Pathogenic Yeasts

Image-based quantification of *Candida albicans* filamentation and hyphal length using the open-source visual programming language JIPipe

Jan-Philipp Praetorius [1,†], Sophia U.J. Hitzler [2,†], Mark S. Gresnigt [2,*], Marc Thilo Figge [1,3,*]

[1]Applied Systems Biology, Leibniz Institute for Natural Product Research and Infection Biology – Hans Knöll Institute (HKI), 07745 Jena, Germany
[2]Junior Research Group Adaptive Pathogenicity Strategies, Leibniz Institute for Natural Product Research and Infection Biology – Hans Knöll Institute (Leibniz-HKI), 07745 Jena, Germany
[3]Institute of Microbiology, Faculty of Biological Sciences, Friedrich Schiller University Jena, 07745 Jena, Germany
*Corresponding authors. Mark S. Gresnigt, Junior Research Group Adaptive Pathogenicity Strategies, Leibniz Institute for Natural Product Research and Infection Biology – Hans Knöll Institute, Adolf-Reichwein-Strasse 23, 07745 Jena, Germany. E-mail: mark.gresnigt@leibniz-hki.de; Marc Thilo Figge, Applied Systems Biology, Leibniz Institute for Natural Product Research and Infection Biology – Hans Knöll Institute, Adolf-Reichwein-Strasse 23, 07745 Jena, Germany. E-mail: thilo.figge@leibniz-hki.de
Editor: [Miguel Teixeira]
†These two authors contributed equally to this work.

Abstract

The formation of hyphae is one of the most crucial virulence traits the human pathogenic fungus *Candida albicans* possesses. The assessment of hyphal length in response to various stimuli, such as exposure to human serum, provides valuable insights into the adaptation strategies of *C. albicans* to the host environment. Despite the increasing high-throughput capacity live-cell imaging and data generation, the accurate analysis of hyphal growth has remained a laborious, error-prone, and subjective manual process. We developed an analysis pipeline utilizing the open-source visual programming language Java Image Processing Pipeline (JIPipe) to overcome the limitations associated with manual analysis of hyphal growth. By comparing our automated approach with manual analysis, we refined the strategies to achieve accurate differentiation between yeast cells and hyphae. The automated method enables length measurements of individual hyphae, facilitating a time-efficient, high-throughput, and user-friendly analysis. By utilizing this JIPipe analysis approach, we obtained insights into the filamentation behavior of two *C. albicans* strains when exposed to human serum albumin (HSA), the most abundant protein in human serum. Our findings indicate that despite the known role of HSA in stimulating fungal growth, it reduces filamentous growth. The implementation of our automated JIPipe analysis approach for hyphal growth represents a long-awaited and time-efficient solution to meet the demand of high-throughput data generation. This tool can benefit different research areas investigating the virulence aspects of *C. albicans*.

Keywords: filamentous growth; hyphal length; microscopy; image analysis; label-free; visual programming; quantitative imaging; infection biology

Introduction

A key attribute that makes *Candida albicans* a successful human pathogen, is its ability to morphologically switch between yeast and filamentous forms (true hyphae and pseudohyphae) (Ernst 2000, d'Enfert et al. 2021, Lopes and Lionakis 2022). The yeast morphology is perceived as vital for commensalism (Pande et al. 2013) and dissemination during systemic infection (Gow et al. 2002, Saville et al. 2003). While recent evidence suggests hyphae also play a role during commensal stages (Liang et al. 2024), this morphology is essential for tissue invasion and escape from the immune system (Gow et al. 2002, Mayer et al. 2013, Austermeier et al. 2020).

The yeast-to-hypha transition is induced by diverse environmental triggers such as serum (Taschdjian et al. 1960), neutral pH (Buffo et al. 1984), physiological human body temperature (Mayer et al. 2013), nutrient depletion (Mayer et al. 2013), *N*-acetyl-D-glucosamine (Simonetti et al. 1974), or elevated CO_2 levels (Mardon et al. 1969), as well as synthetic culture media (Lee et al. 1975). Importantly, over the past years it has become apparent that *C. albicans* induces/potentiates its filamentous growth upon interaction with specific host proteins (Case et al. 2021, Jaeger et al. 2024), thereby adaptively regulating its pathogenicity in response to the host.

Filamentous growth is closely connected to *C. albicans* virulence (Berman and Sudbery 2002). Numerous genes expressed when hyphae are formed contribute to virulence by mediating adhesion (*Als3*, *Hwp1*) (Staab et al. 1999, Phan et al. 2007, Murciano et al. 2012), protease activity (*Sap4-6*) (Naglik et al. 2003, Taylor et al. 2005, Albrecht et al. 2006), toxin production (*Ece1*) (Moyes et al. 2016), and defense against host reactive oxygen species (*Sod5*) (Gleason et al. 2014). Thereby, hyphae formation is crucial for adhesion and host cell invasion (Calderone and Fonzi 2001). While filament initiation is associated with cell wall remodeling that can promote immune recognition, it also facilitates immune evasion (Jaeger et al. 2024). Innate immune cells struggle to phagocytose the growing hyphae, leading to the formation of frustrated phagosomes (Maxson et al. 2018). Initiation of filamentation and

Received 16 December 2024; **revised** 28 February 2025; **accepted** 12 March 2025

elongation of hyphae within the phagosome of macrophages facilitates cellular disruption (Lo et al. 1997, McKenzie et al. 2010, Uwamahoro et al. 2014, Erwig and Gow 2016, Tucey et al. 2020, Westman et al. 2020, Olivier et al. 2022). Macrophages need to fold ingested hyphae to fit them within phagosomes (Bain et al. 2021). Furthermore, the inability to form hyphae results in a loss of candidalysin toxin production and delivery, hindering tissue or immune cell lysis (Birse et al. 1993, Kasper et al. 2018, Ho et al. 2019, Mogavero et al. 2021). To quantify the phagocytosis of fungi, automated image analysis of confrontation assays has proven to be the methodology of choice in various studies (Kraibooj et al. 2014, Mattern et al. 2015, Cseresnyes et al. 2018, 2020, Hassan et al. 2019, 2020, Schmidt et al. 2020).

Due to the multifactorial role of filamentation in host–pathogen interactions, the degree to which filamentation is induced can dictate the outcome of interactions. For this reason, assessment of filamentation remains an important aspect when studying fungal infection biology (Sudbery 2011, Chen et al. 2020, Villa et al. 2020). Nevertheless, quantification of filamentation is laborious. Commonly, microscopy images are examined in open-source software such as ImageJ (Rueden et al. 2017), followed by manual measurement of each fungal cell (Glazier et al. 2018, Oliveira-Pacheco et al. 2018, Tams et al. 2020, Wakade et al. 2023, Sprague et al. 2024). To ensure reliable outcomes, between 50 and 200 fungal cells are assessed per experimental condition (Glazier et al. 2018, Oliveira-Pacheco et al. 2018, Tams et al. 2020). Besides the time involved to perform accurate analysis, manual quantification is susceptible to human error, biases, or fatigue, all of which can influence the results.

Advances in imaging technologies (Cole 2014, Jensen et al. 2015) have enabled visualization of filamentation in high detail and in high-throughput. The combination of image analysis based on fluorescence staining with image-based systems biology approach enables the quantification of the kinetics of hyphal development, hyphal expansion, and epithelial invasion by *C. albicans* (Mech et al. 2014, Medyukhina et al. 2015). Nevertheless, given that fluorescent staining can affect biological function in live-cell analysis (Cseresnyes et al. 2020), is associated with higher costs, staining artefacts, and time investments, label-free analysis is preferred.

The implementation of computer-assisted image analysis can address the limitations of manual filamentation measurements. However, building automated image analysis pipelines requires programming skills. The open source visual programming language Java Image Processing Pipeline (JIPipe: http://www.jipipe.org) (Gerst et al. 2023) enables straightforward development of pipelines. It incorporates the fundamental capabilities of the ImageJ software (Schindelin et al. 2015), and is intended for use by both image analysis experts as well as researchers without prior programming experience.

In our study, we compared manual analysis of images to various novel automated approaches using JIPipe (Gerst et al. 2023). Our objective was to provide a high throughput automated and user-friendly analysis using JIPipe software tool to replace the current manual quantification of filamentation. We subsequently applied our tool to analyze how albumin, the most abundant protein in serum, impacts filamentation. Since serum is a key inducer of filamentation (Taschdjian et al. 1960).

Methods

Strains and culture conditions

Candida albicans strains used in this study were the commonly used wildtype strain SC5314 (Gillum et al. 1984) and the oral isolate 101 (Schonherr et al. 2017). To inoculate cultures, single colonies were picked from yeast peptone dextrose (YPD) agar plates and grown in 5 ml liquid YPD (with 2% peptone) medium using a 25-ml Erlenmeyer glass flask. Cultures were incubated overnight in an orbital shaker at 180 rpm and 30°C. Yeast cells were harvested by centrifugation (20 000 × *g*, 1 min), washed three times with phosphate buffer saline (PBS) pH 7.4, and adjusted to 2×10^7 yeast cells/ml in PBS (pH 7.4).

Live-cell imaging

To visualize the hyphae of the two clinical strains, 1×10^4 yeast cells per well were inoculated in a 96-well plate in PBS (pH 7.4) or RPMI-1640 medium with L-glutamine (RPMI, Thermo Fisher Scientific), supplemented with or without 10 mg/ml human serum albumin (HSA, Sigma). The cultures were imaged using a Cell Discoverer 7 microscope (Zeiss) at 37°C with 5% CO_2. Microscopy images were captured at 10× magnification with different light sources (bright-field, oblique, and phase) every 30 min for 4 h. Images of the 3 h time point were exported with an image size of 3724 × 2690 pixel and a resolution of 0.459 µm × 0.459 µm per pixel.

Manual hyphal measurement

Images were imported into ImageJ 1.54 g software (National Institutes of Health, USA). The distance from the yeast cell to the hyphal tip was measured using the segmented line tool. When fungal cells had branching hyphae, only the primary hypha was measured. Two individual hyphae, with an easily detectable crossing were measured. Yeast cells lacking any indication of germ-tube formation were counted, but not measured. In each experimental setting, all fungal cells were quantitatively assessed in images acquired from two distinct replicates. Fungal clumps or undistinguishable hyphal formation with more than one crossing as well as cells that were not fully visible within the image were excluded (Fig. 1).

Automated image characterization

To implement automated image analysis in a user-friendly tool we used the open source visual programming language JIPipe (http://www.jipipe.org) (Gerst et al. 2023). The use of JIPipe also facilitates a consistent reproduction of the image processing between experiments. The established analysis pipeline can be divided into three distinct compartments: (i) the segmentation of the fungi, (ii) the identification of the morphotypes, and (iii) the measurement of cells exhibiting filamentous growth.

Segmentation of the fungi

The computer-based analysis required transformation (segmentation) of the hyphae imaged in grayscale images into binary images. There are various approaches that can be used for this, each with its own subtleties. Thus, we compared four approaches to segment the fungus. We used two approaches based on classical image analysis. These differ in terms of the operators they use, which are chosen to incorporate as much as possible image features in the final binary image of fungal structures. We further tested ilastik (Berg et al. 2019), a well-established machine-learning-based segmentation tool, and Omnipose (Cutler et al. 2022) a deep learning approach.

We focused our first classical image analysis approach on minimizing the number of image processing steps to achieve segmentation of the fungi, while preventing the introduction of artifacts. This approach was designated as the minimal viable product (MVP). This procedure entailed the removal of the background

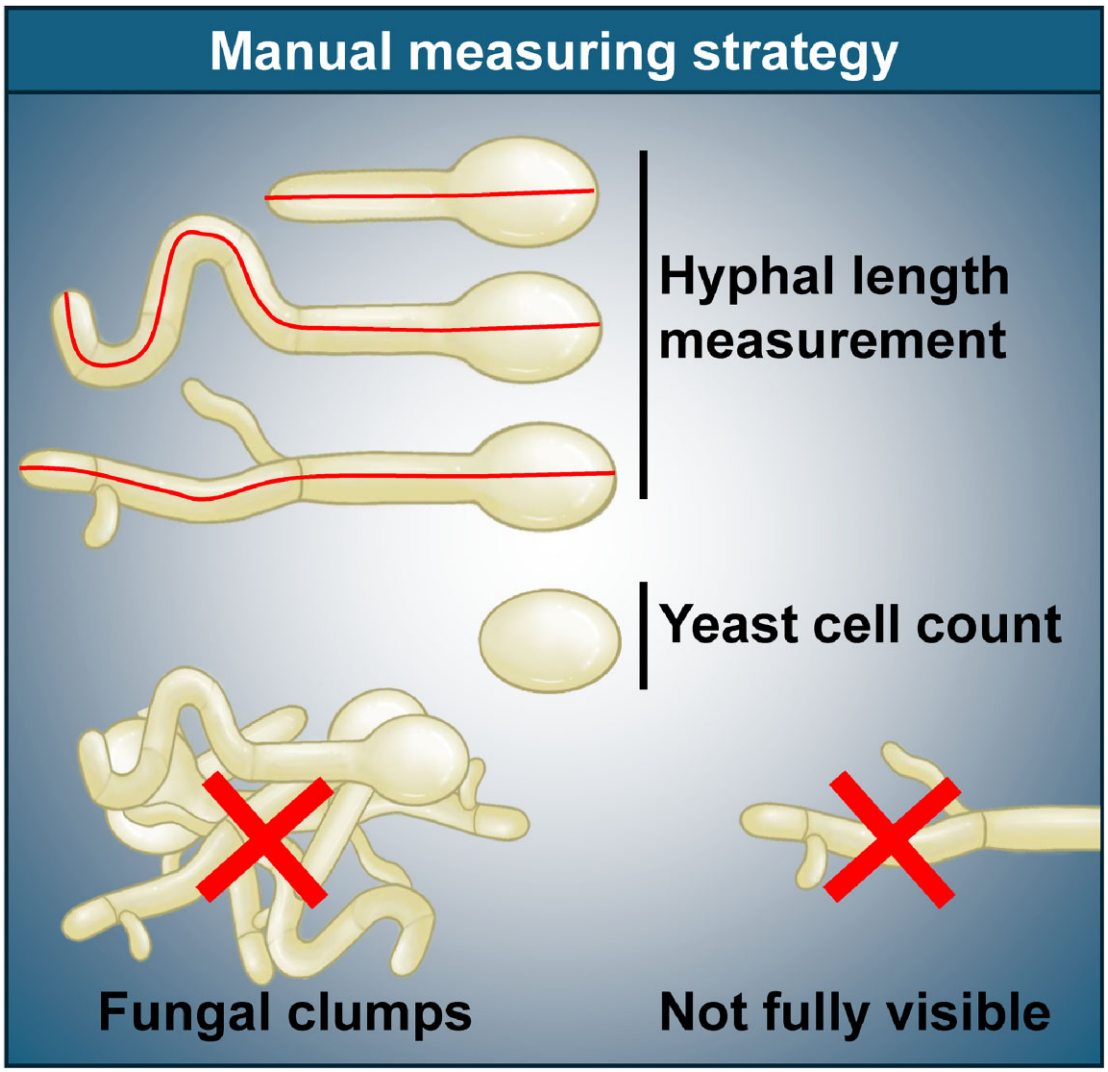

Figure 1. Parameters for manual hyphal length measurement.

signal *via* a rolling-ball or paraboloid algorithm. A filter with a size of 10 pixel was applied, which correlates with the diameter of a yeast cell, whereby all objects smaller than a yeast cell are removed. Subsequently, binarization is conducted with a threshold of 10% of the maximum pixel intensity, with the objective of eliminating "noise" from the image. This optimal threshold level was determined using the intensity histogram, in which only noise and background signals represent 10% of the maximum intensity after the preceding rolling-ball background removal. After transforming the image to a binary image three postprocessing steps were performed: (i) The despeckle operation was performed to remove single pixel artifacts, which smoothes the contour of the binary objects. (ii) Objects smaller than 40 pixels are removed, which in the case of a circle corresponds to a diameter of 3.2 µm, which is smaller than a *C. albicans* yeast cell. (iii) All objects that are connected to the image border were removed. Subsequently, a quantitative characterization is conducted on the binary objects, which represent the contour of *C. albicans* hyphae and yeast cells. The second classical image analysis approach is more advanced and is described in the Supplementary material: *Fungus segmentation using White-Top-Hat algorithm*.

The interactive machine learning-based tool ilastik (Berg et al. 2019) was the third method tested for segmentation. This approach required manual annotation on two replicates for the model training (Fig. S1), which was then applied to all other samples. However, as the training has high computational demands, the training was restricted to only two samples. A key benefit of ilastik is that it provides an immediate insight into the segmentation results through the application of individual markers, which serve as labels for the tool itself (Berg et al. 2019). Annotations of this nature are only required in the context of supervised machine learning tools, with the purpose of demonstrating to the model the knowledge it should acquire. Conversely, classical approaches such as the MVP developed in this study do not necessitate such markers. The segmentation of fungal structures in ilastik was conducted using the pixel classification method, which employed all intensity, edge, and texture features. Prior to this, the image was smoothed using a Gaussian filter, with all of ilastik's available and recommended sigma values (0.7, 1.0, 1.6, 3.5, 5.0, and 10 pixels) to capture as many features as possible.

The fourth method for segmenting the fungus was the deep learning-based segmentation tool Omnipose (Cutler et al. 2022). This tool has been designed for use with elongated or branched cells. One of the two crucial parameters used in this approach is the average object diameter, which was set to 10 pixels (4.5 µm), the average diameter of the hyphae (Sudbery 2011,

Chen et al. 2020, Villa et al. 2020). The second crucial parameter is the selection of the pretrained model, with the *Nucleus* model being the most accurate with regard to the cell contour upon visual inspection. The same postprocessing steps as in the MVP segmentation approach were used.

Identification of the morphotype

Following the generation of binary images of the fungi, the morphotype (yeast or hyphae) of each individual object is identified. In experiments where yeast cells are predominantly present, clusters of yeast cells need to be separated into individual cells in the binary images. At the same time, the splitting of clusters and overlapping filament structures leads to artifacts in experiments with filaments, which affects the reliability of the measurements obtained. To achieve this, we segmented experimental conditions in which no hyphae were present or only a minimal amount. The median value of each binary yeast cell was calculated. Using a histogram, we determined that a threshold value of 250 pixels (112 µm) can effectively distinguishes images with predominantly hyphae from those that have predominantly yeast cells. We separated the cell clusters into their individual yeast using a marker-based watershed algorithm, also referred to as seeded watershed (Soille and Vincent 1990). The number of markers per yeast cell is initially established through the utilization of a Laplacian of Gaussian operator on the original image, which is particularly well-suited for the detection of edges. A kernel radius of seven pixels (3.2 µm, representing the average expected diameter of a yeast cell) was employed. To focus exclusively on the particularly prominent edges of the yeast cells, the output of the Laplacian of Gaussian was taken above a threshold value of 60% of the maximum intensity. To guarantee that solely the markers located within the fungal structure are retained, we ensured that only markers overlapping with the previously segmented fungal masks are included. Subsequently, the seeded watershed operation is performed with the determined markers on the segmented fungus mask (Fig. S2).

Per segmented object distinction between the yeast and hyphae morphotypes is made using a two-parameter filter (Fig. S3A). An object is designated as a yeast if it has a footprint area of <320 pixels corresponding to a diameter of 13.54 µm for a circle, and a circularity value greater than 0.8 (with a value of 1 indicating a perfect circle) (Fig. S3B). These parameters were determined using histograms for all objects, whereby the circularity of yeasts that have just initiated filamentation is in most cases below 0.8. All objects not designated as yeast are automatically designated as hyphae.

Measurement of filamentous structures

The hyphal length measurements were conducted *via* an automated image analysis pipeline in JIPipe, which entails the measurement of filament structures. This measurement was carried out on the previously segmented hyphae as well as on previously split yeast clusters, since yeasts that just initiated filamentation are also included in the measurement. The measurement is performed on the skeleton of each object, which reduces the binary objects to one-pixel-wide representations of their shape. Subsequently, the skeleton of each object is converted into JIPipe's own filament data structure, which was previously successful in quantifying filaments of the bacterium *Klebsiella pneumoniae* (Ruhland et al. 2024). To obtain accurate measurements of the individual hyphae over their entire length from the mother cell to the tip of the hyphae, the average radius of a yeast (from the yeast masks) was considered in the measurement process. The final measurement of the filament structure takes place after the moving average has been formed on it. The moving average is formed over three consecutive pixels along the linear filaments, thereby approximating the realistic course of these structures. Furthermore, the downscaling of individual positions along the filament structure also serves to reduce any remaining distortions along the filaments. Prior to the measurement of the hyphae the overlapping filaments of distinct cells are distinguished and branches of individual fungal cells are excluded (Fig. 1). This process is of great importance to avoid the creation of artifacts for an individual hypha, thus preventing the distortion of the hyphal length distribution. This was used to set the parameter connecting possible candidates of nodes at a filament intersection was set to 17 pixels (7.65 µm) to receive as much as possible proper connections among two filament structures. This was employed to identify potential candidates for overlapping filaments. In order to identify the four points of two intersecting filament structures, the distance between the opposite points was set to 17 pixels (7.65 µm). To ensure a consistent comparison between the automated processing and manual measurements, only the longest filaments connected with the yeast cell were measured for each hypha. Subsequently, the filaments were measured, and those shorter than 10 µm were excluded from the analysis. This value was selected as in the early filament initiation stage hyphal length also cannot be accurately quantified using a manual approach, as the germlings are difficult to distinguish from budding yeast.

Analysis with ImageJ plugin AnaMorf

The automated analysis of filaments in fungi is not a novel concept; it was already approached in 2009 with the development of the AnaMorf tool (Barry et al. 2009) for ImageJ. This tool facilitates the characterization of filamentous fungal growth, along with characteristics such as projected area, circularity, total hyphal length, number of hyphal tips, hyphal growth unit, lacunarity, and fractal dimension. We used the AnaMorf tool (Barry et al. 2009) to compare its performance with our newly established JIPipe hyphae analysis pipeline.

Performance measurements and statistical data analysis

To ensure the validity of the automated quantification of filamentous growth initiation and hyphal length in JIPipe, we compared the automated measurements with manual measurements on the same images. The number of data points between manual measurements and the automated analysis, were compared using the Pearson product-moment correlation coefficient. In addition, to the comparison at the distribution level, a validation was also conducted at the object level. To this end, all objects processed by the MVP segmentation from each test condition were evaluated to assess the extent to which they were recognized by the automated process. Given the inherent difficulty in establishing connections between overlapping filaments of distinct hyphal cells, a comprehensive examination was conducted to assess the integrity of the connections formed by each single crossing hypha from the various experimental conditions. For these comparisons at the object level, the accuracy, F-1 score, precision, and recall could then be calculated using the classic metrics of true positives (TP), type 1 error (false positives, FP), and type 2 error (false negatives, FN). The metric precision refers to the extent of the type 1 error ($P = TP/TP + FP$) and recall refers to the extent of the type

2 error (R = TP/TP + FN). The F-1 score provides a metric that includes both errors (F-1 = 2 × (precision × recall)/(precision + recall)).

Statistical comparisons were not only made between the manual and automated hyphal length measurements, but also to what extent statistical differences exist within the respective experimental conditions. Subsequently, these comparisons were contrasted for the manual measurements and the MVP segmentation approach.

Statistical analyses were performed using "SciPy" library in Python, version 1.5.3. Two different comparisons were made within this study with (i) the comparison between the manual and automated quantification, with regard to the different automated analysis approaches, and (ii) the comparison between HSA-treated and nontreated conditions were determined using unpaired two-tailed *t*-tests. The effect size (d) was calculated as defined by Cohen (1992). The ranges of effect size magnitudes are referred to as negligible for $|d| < 0.2$, small for $|d| < 0.5$, medium for $|d| < 0.8$, and large for $|d| \geq 0.8$.

Results

Development and optimization of automated quantification

To verify the rigor of our pipeline to automatically quantify filamentous growth initiation and hyphal length, we first determined whether the automated analysis could identify all fungi within the image. The vast majority of fungi were successfully recognized using the MVP approach (accuracy of 96%, an F-1 score of 96%, a precision of 93%, and a recall of 99%), with only a few artifacts that could not be assigned to a fungus in the original image. A visual inspection of the other image segmentation approaches, suggest a comparable level of performance.

Subsequently, we tested the automated pipeline for (i) its capacity to differentiate yeast from hyphae, (ii) its accuracy in length measurements, and (iii) the extent to which individual crossing hyphae could be measured correctly.

Automated quantification allows for identification of the morphotype

As a first step in the development of our automated analysis tool, different segmentation approaches were compared for their efficiency to assign yeast and hyphae morphology. The Pearson correlation coefficient between the manual measurements and the different segmentation approaches showed significant correlations (*P*-value < .001) for all approaches, yet highlights the best performance of the MVP approach ($r = 0.958$), followed by the white-top-hat (WTH; $r = 0.957$), Omnipose ($r = 0.887$), and ilastik ($r = 0.848$) (Fig. 2A). With the MVP segmentation approach showing the best correlation with manual measurements, we examined this approach in detail regarding the number of yeast and hyphae quantified. Particularly, we checked whether the automated image analysis tends to yield false positive detected yeast cells and false negative detected hyphae across experimental conditions (Fig. 2B).

We observed that the automated analysis falsely identifies some objects as yeast cells. This can be attributed to a number of factors. The segmentation may introduce a gap in between the yeast cell and its corresponding attached hyphae. In this instance, cells that induced filamentation were falsely identified as yeast cells, while the isolated corresponding hyphae measured <10 µm and was excluded, leading to an under detection of hyphae. The MVP segmentation was applied as the best performing approach for the quantification of filament initiation (Fig. 3).

A second dataset was used to evaluate the segmentation approaches in the same manner and revealed the best performance of the MVP and WTH segmentation approaches (Fig. S4). This time WTH demonstrated the strongest correlation with manual annotation ($r = 0.973$), followed by MVP ($r = 0.915$), ilastik ($r = 0.812$), and Omnipose, which exhibited a considerable discrepancy and even negatively correlated ($r = -0.263$). Except for Omnipose, all segmentation approaches show a significant correlation with each other compared to manual annotation.

Morphology annotations using the MVP and WTH segmentation approaches showed best performance on the first and second evaluations, respectively. These methods exhibited only slight discrepancies and with the comparisons being essentially the same. Therefore, the evaluation of automated analysis performance was continued with only the MVP method.

Reliable measurements of cells that exhibit filamentous growth

We tested five distinct automated methodologies to accurately measure the length of hyphae, and compared this to manual measurements. We used the previously published ImageJ plugin AnaMorf (Barry et al. 2009) as well as the different segmentation approaches (MVP, WTH, ilastik, and Omnipose) implemented in JIPipe. Our different approaches only differed in the segmentation of the fungi, which can result in differences in skeletonization and the final measurement of the hyphae. Experimental conditions used were the two different *C. albicans* strains (101 and SC5314) in RPMI culture medium or PBS, and in the presence or absence of HSA. This resulted in eight comparisons across all experimental conditions of each automated approach with the corresponding manual measurements (Fig. 4A). Since MVP segmentation achieved the best results, the detailed hyphae measurements were individually shown for all conditions (Fig. 4B) in the proof of principle section.

To be optimally implemented in the fungal research field, an automated analysis of hyphal length should yield highly similar results as the manual measurements that remain to be the standard in the field. When statistically comparing results coming from the automated analysis pipelines with manual measurements, the MVP approach showed the best performance (Fig. 4A). Not a single comparison was a significantly different from manual measurements, with a median *P*-value < .35 across the eight comparisons. The smallest *P*-values (.09 and .15) were obtained in the condition with SC5314 and 101 grown in PBS in the presence of HSA, respectively. As very poor filamentation was observed in PBS (Fig. S5A), this highlights the limitations of the automated image analysis to accurately measure hyphae grown under poor filamentation-inducing conditions.

We observed that the automated analysis identified isolated outliers for longer measured filaments in the experiments performed with RPMI medium. However, statistical tests show that this phenomenon is statistically negligible under the RPMI conditions, with *P*-values ranging from .31 to .69 and effect sizes below 0.2.

When comparing the automated analysis approaches on the second test data set, a superior analysis is evident in its minimal number of significant differences compared to the manual measurements. However, in contrast to the eight comparisons included in the initial data set, only six were

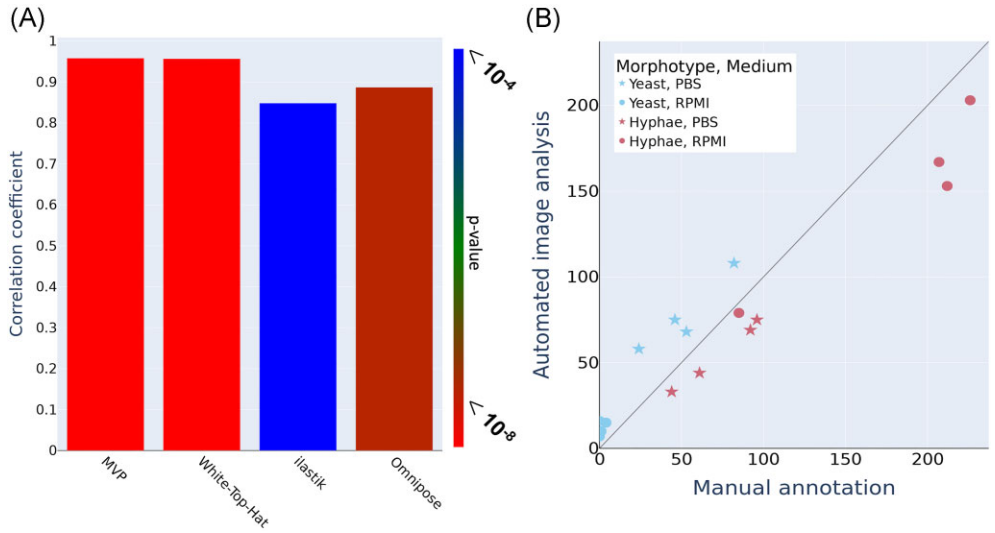

Figure 2. Performance of different segmentation approaches with manual measurements. (A) The correlation coefficient of the number of yeasts and hyphae obtained for all segmentation approaches automated in JIPipe, each compared with the manual annotations. (B) Correlation of the yeast and hyphae annotations by the automated image analysis pipeline applied with the MVP segmentation approach versus manual annotation of yeast and hyphae. Each data point represents the number of corresponding yeast or hyphae cells identified per experimental condition.

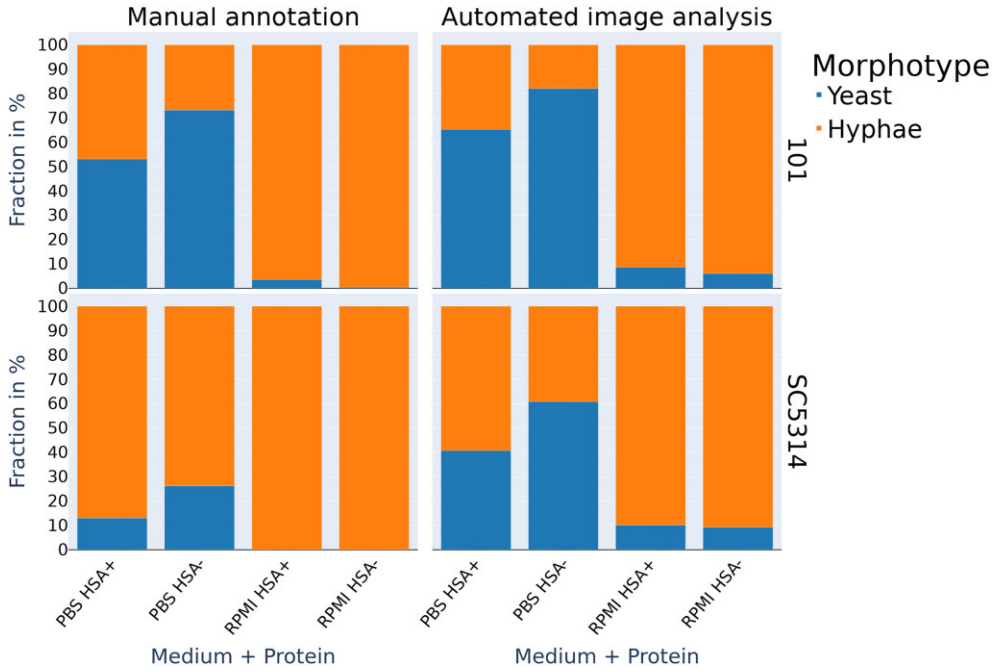

Figure 3. Comparison of the annotation of yeasts and hyphae between manual and automated MVP analysis. Annotation of yeast and hyphae morphology in different conditions expressed as fraction of total identified objects. Experimental conditions represent *C. albicans* grown in PBS or RPMI in the presence or absence of HSA (10 mg/ml, $n = 4$).

conducted, as no hyphae were measured in the PBS experiments lacking albumin (HSA-). The ilastik, MVP, and Omnipose approaches each exhibit two instances of nonsignificant differences. In the validation of the second data set, WTH demonstrated the greatest performance, exhibiting four nonsignificantly different comparisons between the respective conditions (Fig. S4B).

Collectively, automated quantification using classical image processing methods, such as MVP and WTH, can be used to measure the length of hyphae, which are statistically equivalent to the results manual measurements.

Single crossings correction for enhanced hyphae quantification

A particular challenge in measuring hyphae using automated analysis is the accurate measurement of those hyphae that cross each other. During the hyphal growth, branches can be formed by individual hyphae and different hyphae can also overlap when growing closely together. We aimed to accurately identify and quantify filaments in which a maximum of two different hyphae cross at a maximum of one point, as these hyphae are also manually measured without difficulty. In each automated analysis

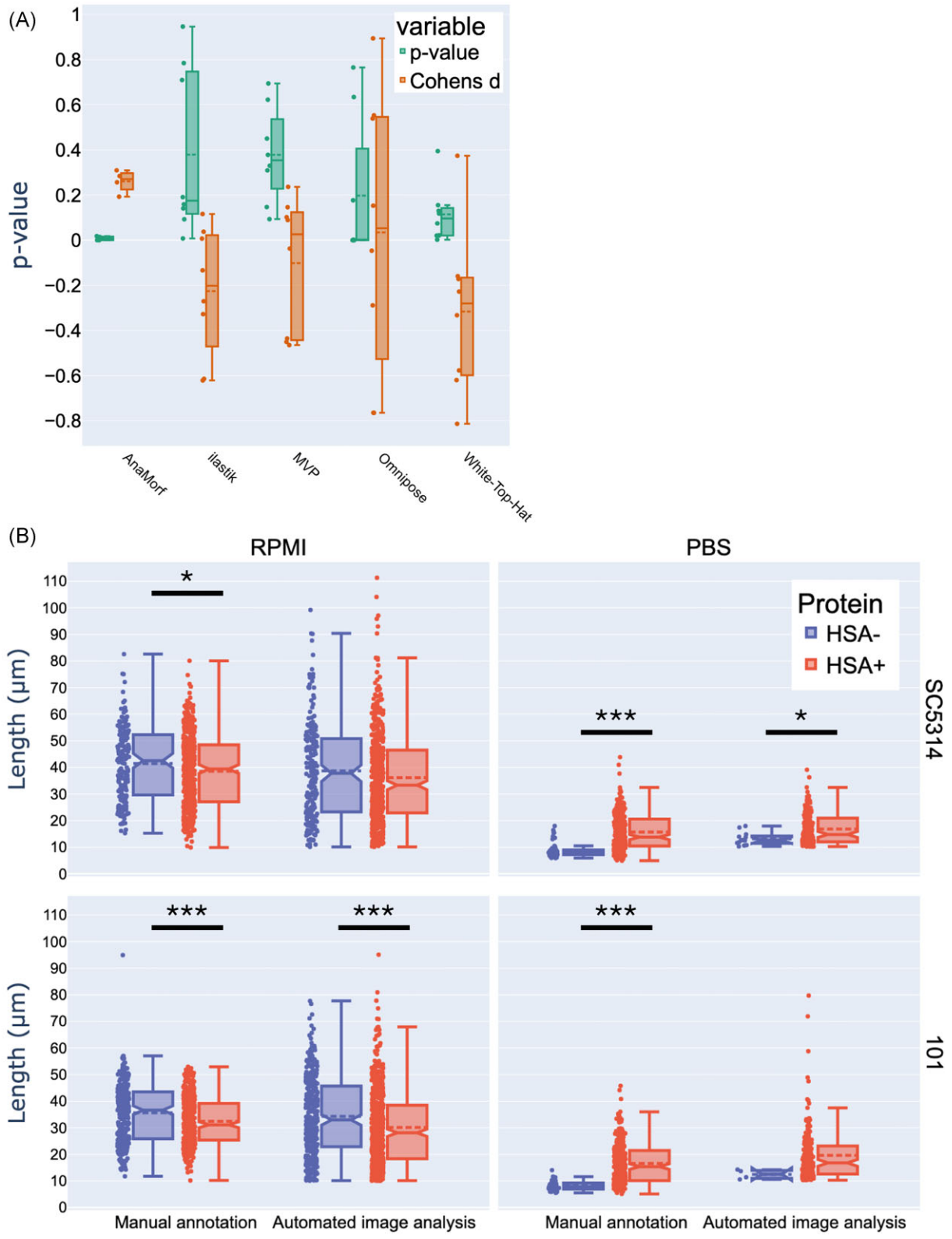

Figure 4. Comparison of hyphal lengths measurements made using automated analysis pipelines and manual measurements. (A) Statistical comparisons of all automated analysis approaches and manual measurements. In the different graphs each data point represents the *P*-value or Cohens d effect size of the comparison of hyphal lengths measured using automated analysis with the corresponding manual measurements across all experimental conditions. (B) A comparison of the hyphal length measurements between the MVP segmentation method and the manual measurements across individual experimental conditions. * = *P*-value < .05, ** = *P*-value < .01, and *** = *P*-value < .001.

we determined whether such intersecting hyphae were correctly measured. As the MVP analysis has thus far demonstrated the greatest reliability, only this approach was validated. An accuracy of 69%, an F-1 score of 82%, precision of 69%, and recall of 100% were determined. Thus, the MVP segmentation tends to yield more single crossings than were actually present, but also generally did not miss any crossings (Fig. 5A). Furthermore, JIPipe facilitates the immediate visualization of the length of each individually measured hypha in its immediate vicinity of the object in the original image (Fig. 5B).

Proof of principle: application to determine filamentation initiation and hyphal length

To compare our automated with manual analysis, we determined the biological effect of HSA on the filamentation initiation and hyphal length of *C. albicans* strains. In RPMI culture medium (filamentation-inducing conditions) the presence of albumin did not significantly impact filamentation ratio as assessed by both methods (Fig. 3). In contrast, in PBS the presence of HSA was manually quantified to significantly induce filamentation [Fig. 3; P-value < .006, Cohen's d (d) = 2.0 for strain 101, and P-value < .01, d = 1.8 for strain SC5314]. With the automated analysis pipeline the same result was obtained [Fig. 4B; P-value < .006, Cohen's d (d) = 2.0 for strain 101, and P-value < .01, d = 1.8 for strain SC5314]. Contrarily, the hyphal length in presence of albumin was found significantly reduced in RPMI as determined by manual measurements (P-value < .0001, d = −0.32 for strain 101) and the automated approach (P-value < .0001, d = −0.3 for strain 101; Fig. S6 and Fig. 4B). In conclusion, when comparing experimental conditions, it can be observed that the same result could be obtained when either using the manual or automated MVP approach.

Discussion

The improvement of techniques for fast, standardized, and unbiased microscopic image analysis is essential to meet the ever-increasing throughput capacity of microscopy systems. We developed an analysis pipeline for measurement of *C. albicans* filamentation and hyphal lengths, which uses the easy-access and open source software JIPipe (Gerst et al. 2023), offering time-efficient, high-throughput, and user-friendly alternative to manual measurements. Moreover, the use of the visual programming language JIPipe opens up accessibility to researchers without programming experience.

Automated image analysis enables researchers to generate and reproduce more accurate and standardized data, facilitating the study of fungal morphology. Numerous methodologies enable quantification and measurement of fungal growth and biofilm formation, such as counting colony forming units (Tessler et al. 1992, Ene et al. 2013, Rossoni et al. 2015, Austermeier et al. 2021, Alonso-Roman et al. 2022, Karkowska-Kuleta et al. 2023, Jaeger et al. 2024), evaluating changes in optical density (Maidan et al. 2008, Rueda et al. 2014, Cui et al. 2016, Austermeier et al. 2021, Dunker et al. 2021, Karkowska-Kuleta et al. 2023, Jaeger et al. 2024), utilizing staining techniques with crystal violet (Jin et al. 2003, Alonso-Roman et al. 2022), or employing flow cytometry (Lynch et al. 1993, McMahon et al. 2023). Particularly, quantification of hyphal length pose challenges. The use of scoring systems, wherein distinct stages of the filamentation process are assigned specific values offers an alternative approach to manual measurements (Azadmanesh et al. 2017, Rossoni et al. 2018, Wakade et al. 2021, 2022). While scoring systems can speed up analysis, the assigned values are approximations, leading to a subjective semiquantitative assessment (Bettauer et al. 2022). Due to its reliance on estimations on an ordinal scale, subtle differences in hyphal lengths are disregarded, resulting in the loss of information within a dataset. Cutting-edge quantitative imaging approaches with automated analysis based on deep learning are a step forward in rapid analysis of morphology, biofilm formation, and filamentation of *C. albicans* (Wurster et al. 2019, Bettauer et al. 2022). To distinguish between the diverse *C. albicans* morphologies, the deep learning tool Candescence was developed (Bettauer et al. 2022). Through implementing an innovative cumulative curriculum-based learning approach, Candescence differentiates nine distinct morphological variations of *C. albicans*, ranging from yeast to complex filamentous structures. Candescence was applied to enable a mutant library screening aimed at identifying genes regulating filamentation within macrophages (Case et al. 2023). Yet, Candescence does not facilitate measurement of hyphal length (Bettauer et al. 2022). Also, other deep learning approaches can facilitate automated analysis of filamentous fungi. NeuroTrack is a processing framework originally designed measure growth and branching of neurons imaged using the Incuyte (Sartorius) live-cell analysis system. Yet, the potential of this tool was recognized and repurposed to quantify fungal growth and morphology (Wurster et al. 2019). Despite the diverse applications of this tool, its exclusive to the Incucyte live-cell analysis system, limiting its accessibility within the scientific community. Moreover, the output of overall fungal hyphal length per square millimeter, as opposed to lengths of individual hyphae, excludes its potential to analyze heterogeneity in the fungal population. Hence, the need for systems allowing automated hyphal length measurements remains.

We identified the open-source visual programming language JiPipe (Gerst et al. 2023) as a platform to design a complex automated filamentation analysis pipeline, while keeping it accessible for researchers without programming experience. As quantitative measurements in automated analysis are performed on binary images the segmentation approach used to get from the original microscopy analysis to the binary images crucially determines the quality of analysis. We compared two classical image processing approaches, namely MVP and WTH, with two based on machine learning and deep learning methods, namely ilastik (Berg et al. 2019) and Omnipose (Cutler et al. 2022). Visual inspection of the Omnipose segmentation revealed that this method consistently produces fragments within fungal hyphae, which impairs its ability to accurately quantify their length. A potential explanation for the poor segmentation relative to classical segmentation approaches is that the segmentation of the fungal structure is typically coarser. The machine learning-based tool ilastik did not show this limitation, and has the advantage that it is directly integrated in JIPipe. Further it allows rapid and efficient adaptations to diverse light and contrast conditions through an interactive training process. The ability to adapt to previously unseen data was apparent when we validated on a second test dataset, where ilastik performed marginally worse results than the best performing WTH quantification on this dataset. This makes ilastik a suitable solution for analyzing *C. albicans* and filamentous structures in general, such as rod-shaped bacteria, within the user-friendly interface of JIPipe.

The two classical segmentation approaches showed the best performance in terms of achieving similar data as the manual hyphal length analysis. A direct comparison of the two approaches revealed that MVP showed better performance over WTH in measuring the length of hyphae. As WTH uses more operations and intermediate steps during segmentation, there is a greater potential

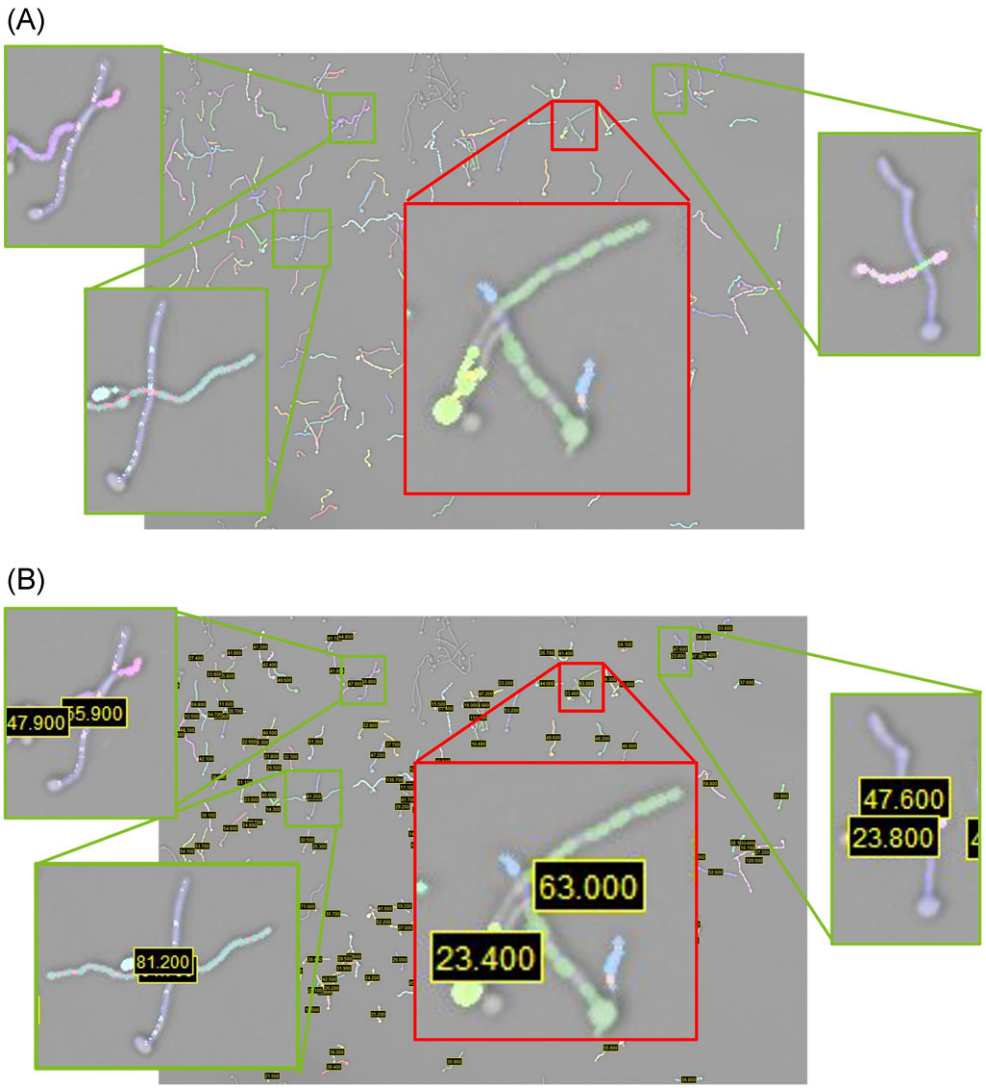

Figure 5. Embedded visualization of the recognized filament structures in JIPipe. (A) Each color overlaid on a hyphen encodes a filament uniquely assigned to an object and thus the assignment of the structures to the objects is indicated by this color coding. In the green-framed windows, the crossing hyphae were correctly assigned, while the assignment in the red-framed window was incorrect. (B) In addition, the lengths of each measured filament structure can be displayed in the representation of (A).

of introducing artifacts and generating errors. However, a more straightforward approach can also constrain the capacity to capture complex aspects within the image. In the evaluation of our second test data set, the WTH performed better than MVP in the measurement of hyphal length and yeast–hyphal differentiation. Highlighting that subtle differences in datasets can influence performance of these two best performing datasets. Despite the fact that classic methods are subject to a threshold value procedure in which parameters must be determined manually and adjusted if necessary, the great advantage of both methods in conjunction with JIPipe is that such parameters can easily be adjusted and the results can be evaluated in the preview integrated in JIPipe.

Previously the ImageJ plugin AnaMorf (Barry et al. 2009) was developed for the characterization of fungal hyphae, offering the possibility of determining a number of filament characteristics. However, we observed that AnaMorf expressed difficulties in distinguishing between these characteristics and measuring them accurately, particularly when there is a high density of fungal cells in the image.

Collectively, from the pipelines we developed, those using MVP or WTH segmentation achieve results similar to manual analysis.

An inherent difficulty of hyphal length measurements is the ability to measure crossing filaments. While manual measurements disregard larger groups or hyphae that are difficult to distinguish, straightforward crossing hyphae can be accurately measured. Excluding, such crossings in automated analysis will result in a loss of data. A step toward capturing these crossing hyphae would be to trace to which yeast cells the hyphae belong to. Yet,s this requires images at different timepoints and far more complicated analysis pipelines. Thus, the detection of crossing remains an unresolved difficulty, particularly in the context of high cell density. Furthermore, the potential of hyphae from *C. albicans* and other filamentous fungi to form branches introduces an additional layer of complexity to the automated hyphal measurements. This represents an optimal point from which to launch further development of automated quantification.

Apart from hyphae, *C. albicans* can form pseudohyphae as an alternative filamentous morphology. The analysis pipeline established in this paper cannot distinguish between the

filamentous hyphal and pseudohyphal morphotypes. When a homogenous morphology shift is induced, the experimenter can make a call based on specific features such as different septa distribution (Sudbery 2001) and a different width (Chen et al. 2020). It is, however, challenging a heterogenous mixture of true hyphae and pseudohyphae is induced. To setup an analysis pipeline that can differentiate between true hyphae and pseudohyphae, further data, particularly from pseudo-hyphae, is required. It would be crucial to distinguish the ratio between filament width and length in order to make a proper distinction. The incorporation of additional steps in the analysis pipeline to distinguish filamentous morphotypes in the future will offer further additional significant opportunity for using automated quantification.

A benefit of our established analysis pipeline in JIPipe is that it allows users, regardless of their computer expertise, to change crucial parameters of the image analysis in a comprehensive and accessible format (Gerst et al. 2023). This enables adaption of the pipeline to specific datasets, like for example hyphae of other pathogenic fungi. The MVP segmentation method is particularly advantageous for adaptation by nonexperts, as the segmentation process is more comprehensible and sources of error can be more readily identified than when using more complex approaches such as WTH. In the context of adapting the analysis pipeline to novel data sets, the modified pipeline should be validated against manual measurements to ensure its performance.

Despite in-depth studies into the processes and genes driving filamentous growth, many unresolved issues persist regarding the intricate regulation of morphological transitions (Sudbery 2011, Chen et al. 2020, Villa et al. 2020). Developments in fungal genetic manipulation have led to the establishment of large mutant libraries (Uhl et al. 2003, Noble et al. 2010, Wang et al. 2022). Implementation of our hyphae analysis pipeline would enable the examination large data sets, such as mutant collections (Wang et al. 2022). Previously a collection of 18 000 mutant strains, was screened to identify genes involved in filamentation using a scoring system that is based on the appearance of the mutant colonies grown on different solid media (Uhl et al. 2003). In addition, the increasing focus on clinical *C. albicans* isolates has accentuated the importance of comprehending the variability in filamentation (Wakade et al. 2021, Brandquist et al. 2023). Implementation of an automated image analysis pipeline like presented in our study could stream-line the process and improve the quantity and quality of data that can be obtained from screening mutant and clinical strain libraries.

The elucidation of filamentation in the context of host–fungal interactions is complex, but can give insights in how *C. albicans* adapts to particular host niches and recognizes favorable conditions for infection (Wartenberg et al. 2014, O'Meara et al. 2015, Case et al. 2021, Wakade et al. 2022, Jaeger et al. 2024). An important aim in development of therapeutics are strategies that limit virulence, so-called antivirulence therapies (Siscar-Lewin et al. 2019). Given the increasing importance of high throughput screening for novel antifungal or antivirulence drugs (Siles et al. 2013, Ajetunmobi et al. 2023, Song et al. 2023), rapid automated analysis of extensive data sets is a valuable asset.

To contribute to the understanding of how environmental cues inflict filamentation, we used our automated approach to show how albumin influences filamentation and hyphal length. Serum is recognized for its ability to induce filamentation (Taschdjian et al. 1960, Shapiro et al. 2011, Sudbery 2011). Albumin is by far the most abundant protein and fulfills multiple roles within the human body (Friedberg 1975, van der Vusse 2009, Taverna et al. 2013, Merlot et al. 2014, Pinsky et al. 2020). Albumin was shown to increase growth of *Candida* species (Austermeier et al. 2021, Pekmezovic et al. 2021), and promote germination and hyphal growth in *Aspergillus fumigatus* (Rodrigues et al. 2005), yet the impact on *C. albicans* filamentation induction and extension remains unclear. With both our automated and manual hyphae analysis, we made the observation that albumin promoted filamentation under nutrient-depleted conditions, yet reduced hyphal length in rich medium. The induction of filamentation may be attributed to albumin providing essential nutrients like iron to *C. albicans* (Pinsky et al. 2020). The upregulation of numerous iron acquisition genes during hyphal elongation emphasizes how closely connected iron acquisition and hyphal formation are (Luo et al. 2021). Albumin also is the main fatty acid binding protein in the plasma (Fitzpatrick et al. 1984, Petitpas et al. 2001, van der Vusse 2009). Albumin can bind prostaglandin E_2 [110], which was shown to induce *C. albicans* filamentation (Kalo-Klein and Witkin 1990). Albumin itself has the potential to serve as a nutrient source (Naglik et al. 2003, Staib 1965, Hube et al. 1994, Martinez and Ljungdahl 2005, Kragh-Hansen 2018) following degradation by *C. albicans* secreted aspartic proteases (Naglik et al. 2003, Hube et al. 1994, 1997, Brunke and Hube 2013). As human serum comprises proteins, lipoproteins, globulins, lipids, hormones, electrolytes, and various other components (Psychogios et al. 2011), its filamentation—inducing potential likely relies on a complex combination of factors. GlcNac, a monosaccharide found in the human serum, stimulates *C. albicans* hyphal growth (Simonetti et al. 1974) by activating the Ras1-cAMP/PKA signaling pathway (Du et al. 2020). Serum contains α1-antitrypsin, which can increase filamentation in a dose dependent manner (Jaeger et al. 2024). A serum fractionation study revealed that the highest filamentation induction was achieved with a fraction composed for 98% of albumin (Barlow et al. 1974). Yet, further fractionation pinpointed a lower-molecular-weight compound of unknown identity. Collectively, many components of the human serum differentially impact *C. albicans* filamentation induction and hyphal growth.

Our study designed and implemented an automated image analysis pipeline in JIPipe, which is based on the well-established ImageJ software. Our approach, significantly enhancing the efficiency and accuracy of measuring hyphal lengths in *C. albicans*. Our approach provides a future orientated solution that implements unbiased, accurate, reproducible, accessible, label-free and high-throughput analysis of filamentation. By applying the automated analysis next to manual measurements, we show that both methods yielded the same observation that human albumin reduces filamentation. Our findings underscore the importance of integrating advanced computational methods in fungal research to standardize the filamentation read-out throughout laboratories worldwide.

Acknowledgments

We acknowledge Salomé LeibundGut-Landmann (Section of Immunology, Vetsuisse-Faculty, University of Zurich) for providing the 101 strain. We thank Nikshitha Tulasi, and Ceren Oktay (Adaptive Pathogenicity Strategies, Leibniz-HKI) for experimental support.

Supplementary data

Supplementary data is available at *FEMSYR Journal* online.

Conflict of interest: The authors declare no competing interests.

Funding

S.U.J.H. and M.S.G. were funded by the Deutsche Forschungsgemeinschaft (DFG, German Research Foundation) Emmy Noether Program (project number 434385622/GR 5617/1-1) to M.S.G. This research was supported by the Free State of Thuringia and co-funded by the European Union—Project-ID 2023 FGI 0004. "A Live broadcast of the interactions between host and fungal pathogens" to M.S.G. M.S.G. and M.T.F. are further supported by the DFG within the Collaborative Research Centre (CRC)/Transregio (TRR) 124 "FungiNet" projects C1 and B4 (DFG project number 210879364). Further funding was provided to M.T.F. by the Deutsche Forschungsgemeinschaft under Germany's Excellence Strategy—EXC 2051: Balance of the Microverse—Project-ID 390713860.

Data availability and software

All data is available for download here:
https://asbdata.hki-jena.de/PraetoriusEtAl2024_filamentation
The software versions of the used tools such as JIPipe (www.jipipe.org) is 3.0.0 (Gerst et al. 2023) and for ilastik (www.ilastik.org) (Berg et al. 2019) the version 1.3.3.

References

Ajetunmobi OH, Wall G, Vidal Bonifacio B *et al.* High-throughput screening of the repurposing hub library to identify drugs with novel inhibitory activity against *Candida albicans* and *Candida auris* biofilms. *J Fungi* 2023;**9**:879. https://doi.org/10.3390/jof9090879.

Albrecht A, Felk A, Pichova I *et al.* Glycosylphosphatidylinositol-anchored proteases of *Candida albicans* target proteins necessary for both cellular processes and host-pathogen interactions. *J Biol Chem* 2006;**281**:688–94. https://doi.org/10.1074/jbc.M509297200.

Alonso-Roman R, Last A, Mirhakkak MH *et al. Lactobacillus rhamnosus* colonisation antagonizes *Candida albicans* by forcing metabolic adaptations that compromise pathogenicity. *Nat Commun* 2022;**13**:3192. https://doi.org/10.1038/s41467-022-30661-5.

Austermeier S, Kasper L, Westman J *et al.* I want to break free—macrophage strategies to recognize and kill *Candida albicans*, and fungal counter-strategies to escape. *Curr Opin Microbiol* 2020;**58**:15–23. https://doi.org/10.1016/j.mib.2020.05.007.

Austermeier S, Pekmezovic M, Porschitz P *et al.* Albumin neutralizes hydrophobic toxins and modulates *Candida albicans* pathogenicity. *mBio* 2021;**12**:e0053121. https://doi.org/10.1128/mBio.00531-21.

Azadmanesh J, Gowen AM, Creger PE *et al.* Filamentation involves two overlapping, but distinct, programs of filamentation in the pathogenic fungus *Candida albicans*. *G3* 2017;**7**:3797–808. https://doi.org/10.1534/g3.117.300224.

Bain JM, Alonso MF, Childers DS *et al.* Immune cells fold and damage fungal hyphae. *Proc Natl Acad Sci USA* 2021;**118**. https://doi.org/10.1073/pnas.2020484118.

Barlow AJ, Aldersley T, Chattaway FW. Factors present in serum and seminal plasma which promote germ-tube formation and mycelial growth of *Candida albicans*. *J Gen Microbiol* 1974;**82**:261–72. https://doi.org/10.1099/00221287-82-2-261.

Barry DJ, Chan C, Williams GA. Morphological quantification of filamentous fungal development using membrane immobilization and automatic image analysis. *J Ind Microbiol Biotechnol* 2009;**36**:787–800. https://doi.org/10.1007/s10295-009-0552-9.

Berg S, Kutra D, Kroeger T *et al.* ilastik: interactive machine learning for (bio)image analysis. *Nat Methods* 2019;**16**:1226–32. https://doi.org/10.1038/s41592-019-0582-9.

Berman J, Sudbery PE. *Candida albicans*: a molecular revolution built on lessons from budding yeast. *Nat Rev Genet* 2002;**3**:918–31. https://doi.org/10.1038/nrg948.

Bettauer V, Costa A, Omran RP *et al.* A deep learning approach to capture the essence of *Candida albicans* morphologies. *Microbiol Spectr* 2022;**10**:e0147222. https://doi.org/10.1128/spectrum.01472-22.

Birse CE, Irwin MY, Fonzi WA *et al.* Cloning and characterization of ECE1, a gene expressed in association with cell elongation of the dimorphic pathogen *Candida albicans*. *Infect Immun* 1993;**61**:3648–55. https://doi.org/10.1128/iai.61.9.3648-3655.1993.

Brandquist ND, Lampman C, Smith EJ *et al.* Significant variation of filamentation phenotypes in clinical *Candida albicans* strains. *Front Cell Infect Microbiol* 2023;**13**:1207083. https://doi.org/10.3389/fcimb.2023.1207083.

Brunke S, Hube B. Two unlike cousins: *C andida albicans* and *C. glabrata* infection strategies. *Cell Microbiol* 2013;**15**:701–8. https://doi.org/10.1111/cmi.12091.

Buffo J, Herman MA, Soll DR. A characterization of pH-regulated dimorphism in *Candida albicans*. *Mycopathologia* 1984;**85**:21–30. https://doi.org/10.1007/BF00436698.

Calderone RA, Fonzi WA. Virulence factors of *Candida albicans*. *Trends Microbiol* 2001;**9**:327–35. https://doi.org/10.1016/s0966-842x(01)02094-7.

Case NT, Duah K, Larsen B *et al.* The macrophage-derived protein PTMA induces filamentation of the human fungal pathogen *Candida albicans*. *Cell Rep* 2021;**36**:109584. https://doi.org/10.1016/j.celrep.2021.109584.

Case NT, Westman J, Hallett MT *et al.* Respiration supports intraphagosomal filamentation and escape of *Candida albicans* from macrophages. *mBio* 2023;**14**:e0274523. https://doi.org/10.1128/mbio.02745-23.

Chen H, Zhou X, Ren B *et al.* The regulation of hyphae growth in *Candida albicans*. *Virulence* 2020;**11**:337–48. https://doi.org/10.1080/21505594.2020.1748930.

Cohen J. A power primer. *Psychol Bull* 1992;**112**:155–9. https://doi.org/10.1037/0033-2909.112.1.155.

Cole R. Live-cell imaging. *Cell Adh Migr* 2014;**8**:452–9. https://doi.org/10.4161/cam.28348.

Cseresnyes Z, Hassan MIA, Dahse HM *et al.* Quantitative impact of cell membrane fluorescence labeling on phagocytosis measurements in confrontation assays. *Front Microbiol* 2020;**11**:1193. https://doi.org/10.3389/fmicb.2020.01193.

Cseresnyes Z, Kraibooj K, Figge MT. Hessian-based quantitative image analysis of host-pathogen confrontation assays. *Cytometry Pt A* 2018;**93**:346–56. https://doi.org/10.1002/cyto.a.23201.

Cui S, Hassan RY, Heintz-Buschart A *et al.* Regulation of *Candida albicans* interaction with macrophages through the activation of HOG pathway by Genistein. *Molecules* 2016;**21**:162. https://doi.org/10.3390/molecules21020162.

Cutler KJ, Stringer C, Lo TW *et al.* Omnipose: a high-precision morphology-independent solution for bacterial cell segmentation. *Nat Methods* 2022;**19**:1438–48. https://doi.org/10.1038/s41592-022-01639-4.

d'Enfert C, Kaune AK, Alaban LR *et al.* The impact of the fungus-host-microbiota interplay upon *Candida albicans* infections: current knowledge and new perspectives. *FEMS Microbiol Rev* 2021;**45**. https://doi.org/10.1093/femsre/fuaa060.

Du H, Ennis CL, Hernday AD *et al.* N-acetylglucosamine (GlcNAc) sensing, utilization, and functions in *Candida albicans*. *J Fungi* 2020;**6**:129. https://doi.org/10.3390/jof6030129.

Dunker C, Polke M, Schulze-Richter B *et al.* Rapid proliferation due to better metabolic adaptation results in full virulence of a filament-deficient *Candida albicans* strain. *Nat Commun* 2021;**12**:3899. https://doi.org/10.1038/s41467-021-24095-8.

Ene IV, Cheng SC, Netea MG *et al.* Growth of *Candida albicans* cells on the physiologically relevant carbon source lactate affects their recognition and phagocytosis by immune cells. *Infect Immun* 2013;**81**:238–48. https://doi.org/10.1128/IAI.01092-12.

Ernst JF. Transcription factors in *Candida albicans*—environmental control of morphogenesis. *Microbiology* 2000;**146**:1763–74. https://doi.org/10.1099/00221287-146-8-1763.

Erwig LP, Gow NA. Interactions of fungal pathogens with phagocytes. *Nat Rev Microbiol* 2016;**14**:163–76. https://doi.org/10.1038/nrmicro.2015.21.

Fitzpatrick FA, Liggett WF, Wynalda MA. Albumin-eicosanoid interactions. A model system to determine their attributes and inhibition. *J Biol Chem* 1984;**259**:2722–7. https://doi.org/10.1016/s0021-9258(17)43205-4.

Friedberg F. Albumin as the major metal transport agent in blood. *FEBS Lett* 1975;**59**:140–1. https://doi.org/10.1016/0014-5793(75)80360-7.

Gerst R, Cseresnyes Z, Figge MT. JIPipe: visual batch processing for ImageJ. *Nat Methods* 2023;**20**:168–9. https://doi.org/10.1038/s41592-022-01744-4.

Gillum AM, Tsay EY, Kirsch DR. Isolation of the *Candida albicans* gene for orotidine-5'-phosphate decarboxylase by complementation of *S. cerevisiae* ura3 and *E. coli* pyrF mutations. *Molec Gen Genet* 1984;**198**:179–82. https://doi.org/10.1007/BF00328721.

Glazier VE, Murante T, Koselny K *et al.* Systematic complex haploinsufficiency-based genetic analysis of *Candida albicans* transcription factors: tools and applications to virulence-associated phenotypes. *G3* 2018;**8**:1299–314. https://doi.org/10.1534/g3.117.300515.

Gleason JE, Galaleldeen A, Peterson RL *et al. Candida albicans* SOD5 represents the prototype of an unprecedented class of Cu-only superoxide dismutases required for pathogen defense. *Proc Natl Acad Sci USA* 2014;**111**:5866–71. https://doi.org/10.1073/pnas.1400137111.

Gow NA, Brown AJ, Odds FC. Fungal morphogenesis and host invasion. *Curr Opin Microbiol* 2002;**5**:366–71. https://doi.org/10.1016/s1369-5274(02)00338-7.

Hassan MIA, Cseresnyes Z, Al-Zaben N *et al.* The geographical region of origin determines the phagocytic vulnerability of *Lichtheimia strains*. *Environ Microbiol* 2019;**21**:4563–81. https://doi.org/10.1111/1462-2920.14752.

Hassan MIA, Kruse JM, Kruger T *et al.* Functional surface proteomic profiling reveals the host heat-shock protein A8 as a mediator of *Lichtheimia corymbifera* recognition by murine alveolar macrophages. *Environ Microbiol* 2020;**22**:3722–40. https://doi.org/10.1111/1462-2920.15140.

Ho J, Yang X, Nikou SA *et al.* Candidalysin activates innate epithelial immune responses via epidermal growth factor receptor. *Nat Commun* 2019;**10**:2297. https://doi.org/10.1038/s41467-019-09915-2.

Hube B, Monod M, Schofield DA *et al.* Expression of seven members of the gene family encoding secretory aspartyl proteinases in *Candida albicans*. *Mol Microbiol* 1994;**14**:87–99. https://doi.org/10.1111/j.1365-2958.1994.tb01269.x.

Hube B, Sanglard D, Odds FC *et al.* Disruption of each of the secreted aspartyl proteinase genes SAP1, SAP2, and SAP3 of *Candida albicans* attenuates virulence. *Infect Immun* 1997;**65**:3529–38. https://doi.org/10.1128/iai.65.9.3529-3538.1997.

Jaeger M, Dietschmann A, Austermeier S *et al.* Alpha1-antitrypsin impacts innate host-pathogen interactions with *Candida albicans* by stimulating fungal filamentation. *Virulence* 2024;**15**:2333367. https://doi.org/10.1080/21505594.2024.2333367.

Jensen PA, Dougherty BV, Moutinho TJ *et al.* Miniaturized plate readers for low-cost, high-throughput phenotypic screening. *SLAS Technology* 2015;**20**:51–55. https://doi.org/10.1177/2211068214555414.

Jin Y, Yip HK, Samaranayake YH *et al.* Biofilm-forming ability of *Candida albicans* is unlikely to contribute to high levels of oral yeast carriage in cases of human immunodeficiency virus infection. *J Clin Microbiol* 2003;**41**:2961–7. https://doi.org/10.1128/JCM.41.7.2961-2967.2003.

Kalo-Klein A, Witkin SS. Prostaglandin E2 enhances and gamma interferon inhibits germ tube formation in *Candida albicans*. *Infect Immun* 1990;**58**:260–2. https://doi.org/10.1128/iai.58.1.260-262.1990.

Karkowska-Kuleta J, Kulig K, Bras G *et al. Candida albicans* biofilm-derived extracellular vesicles are involved in the tolerance to caspofungin, biofilm detachment, and fungal proteolytic activity. *J Fungi* 2023;**9**:1078. https://doi.org/10.3390/jof9111078.

Kasper L, Konig A, Koenig PA *et al.* The fungal peptide toxin Candidalysin activates the NLRP3 inflammasome and causes cytolysis in mononuclear phagocytes. *Nat Commun* 2018;**9**:4260. https://doi.org/10.1038/s41467-018-06607-1.

Kragh-Hansen U. Possible mechanisms by which enzymatic degradation of Human serum albumin can lead to bioactive peptides and biomarkers. *Front Mol Biosci* 2018;**5**:63. https://doi.org/10.3389/fmolb.2018.00063.

Kraibooj K, Park HR, Dahse HM *et al.* Virulent strain of *Lichtheimia corymbifera* shows increased phagocytosis by macrophages as revealed by automated microscopy image analysis. *Mycoses* 2014;**57**:56–66. https://doi.org/10.1111/myc.12237.

Lee KL, Buckley HR, Campbell CC. An amino acid liquid synthetic medium for the development of mycelial and yeast forms of *Candida albicans*. *Med Mycol* 1975;**13**:148–53. https://doi.org/10.1080/00362177585190271.

Liang SH, Sircaik S, Dainis J *et al.* The hyphal-specific toxin candidalysin promotes fungal gut commensalism. *Nature* 2024;**627**:620–7. https://doi.org/10.1038/s41586-024-07142-4.

Lo HJ, Kohler JR, DiDomenico B *et al.* Nonfilamentous *C. albicans* mutants are avirulent. *Cell* 1997;**90**:939–49. https://doi.org/10.1016/s0092-8674(00)80358-x.

Lopes JP, Lionakis MS. Pathogenesis and virulence of *Candida albicans*. *Virulence* 2022;**13**:89–121. https://doi.org/10.1080/21505594.2021.2019950.

Luo G, Wang T, Zhang J *et al. Candida albicans* requires iron to sustain hyphal growth. *Biochem Biophys Res Commun* 2021;**561**:106–12. https://doi.org/10.1016/j.bbrc.2021.05.039.

Lynch ME, Kukuruga M, Nakeff A *et al.* Flow cytometric analysis of germ tube formation in *Candida albicans*. *Med Mycol* 1993;**31**:367–76. https://doi.org/10.1080/02681219380000471.

Maidan MM, De Rop L, Relloso M *et al.* Combined inactivation of the *Candida albicans* GPR1 and TPS2 genes results in avirulence in a mouse model for systemic infection. *Infect Immun* 2008;**76**:1686–94. https://doi.org/10.1128/IAI.01497-07.

Mardon D, Balish E, Phillips AW. Control of dimorphism in a biochemical variant of *Candida albicans*. *J Bacteriol* 1969;**100**:701–7. https://doi.org/10.1128/jb.100.2.701-707.1969.

Martinez P, Ljungdahl PO. Divergence of Stp1 and Stp2 transcription factors in *Candida albicans* places virulence factors required

for proper nutrient acquisition under amino acid control. *Mol Cell Biol* 2005;**25**:9435–46. https://doi.org/10.1128/MCB.25.21.9435-9446.2005.

Mattern DJ, Schoeler H, Weber J *et al.* Identification of the antiphagocytic trypacidin gene cluster in the human-pathogenic fungus *Aspergillus fumigatus*. *Appl Microbiol Biotechnol* 2015;**99**:10151–61. https://doi.org/10.1007/s00253-015-6898-1.

Maxson ME, Naj X, O'Meara TR *et al.* Integrin-based diffusion barrier separates membrane domains enabling the formation of microbiostatic frustrated phagosomes. *eLife* 2018;**7**. https://doi.org/10.7554/eLife.34798.

Mayer FL, Wilson D, Hube B. *Candida albicans* pathogenicity mechanisms. *Virulence* 2013;**4**:119–28. https://doi.org/10.4161/viru.22913.

McKenzie CG, Koser U, Lewis LE *et al.* Contribution of *Candida albicans* cell wall components to recognition by and escape from murine macrophages. *Infect Immun* 2010;**78**:1650–8. https://doi.org/10.1128/IAI.00001-10.

McMahon CL, Esqueda M, Yu JJ *et al.* Development of an imaging flow cytometry method for fungal cytological profiling and its potential application in antifungal drug development. *J Fungi* 2023;**9**:722. https://doi.org/10.3390/jof9070722.

Mech F, Wilson D, Lehnert T *et al.* Epithelial invasion outcompetes hypha development during *Candida albicans* infection as revealed by an image-based systems biology approach. *Cytometry Pt A* 2014;**85**:126–39. https://doi.org/10.1002/cyto.a.22418.

Medyukhina A, Timme S, Mokhtari Z *et al.* Image-based systems biology of infection. *Cytometry Pt A* 2015;**87**:462–70. https://doi.org/10.1002/cyto.a.22638.

Merlot AM, Kalinowski DS, Richardson DR. Unraveling the mysteries of serum albumin-more than just a serum protein. *Front Physiol* 2014;**5**:299. https://doi.org/10.3389/fphys.2014.00299.

Mogavero S, Sauer FM, Brunke S *et al.* Candidalysin delivery to the invasion pocket is critical for host epithelial damage induced by *Candida albicans*. *Cell Microbiol* 2021;**23**:e13378. https://doi.org/10.1111/cmi.13378.

Moyes DL, Wilson D, Richardson JP *et al.* Candidalysin is a fungal peptide toxin critical for mucosal infection. *Nature* 2016;**532**:64–68. https://doi.org/10.1038/nature17625.

Murciano C, Moyes DL, Runglall M *et al.* Evaluation of the role of *Candida albicans* agglutinin-like sequence (Als) proteins in human oral epithelial cell interactions. *PLoS One* 2012;**7**:e33362. https://doi.org/10.1371/journal.pone.0033362.

Naglik JR, Challacombe SJ, Hube B. *Candida albicans* secreted aspartyl proteinases in virulence and pathogenesis. *Microbiol Mol Biol Rev* 2003;**67**:400–28. https://doi.org/10.1128/MMBR.67.3.400-428.2003.

Noble SM, French S, Kohn LA *et al.* Systematic screens of a *Candida albicans* homozygous deletion library decouple morphogenetic switching and pathogenicity. *Nat Genet* 2010;**42**:590–8. https://doi.org/10.1038/ng.605.

Oliveira-Pacheco J, Alves R, Costa-Barbosa A *et al.* The role of *Candida albicans* transcription factor RLM1 in response to carbon adaptation. *Front Microbiol* 2018;**9**:1127. https://doi.org/10.3389/fmicb.2018.01127.

Olivier FAB, Hilsenstein V, Weerasinghe H *et al.* The escape of *Candida albicans* from macrophages is enabled by the fungal toxin candidalysin and two host cell death pathways. *Cell Rep* 2022;**40**:111374. https://doi.org/10.1016/j.celrep.2022.111374.

O'Meara TR, Veri AO, Ketela T *et al.* Global analysis of fungal morphology exposes mechanisms of host cell escape. *Nat Commun* 2015;**6**:6741. https://doi.org/10.1038/ncomms7741.

Pande K, Chen C, Noble SM. Passage through the mammalian gut triggers a phenotypic switch that promotes *Candida albicans* commensalism. *Nat Genet* 2013;**45**:1088–91. https://doi.org/10.1038/ng.2710.

Pekmezovic M, Kaune AK, Austermeier S *et al.* Human albumin enhances the pathogenic potential of *Candida glabrata* on vaginal epithelial cells. *PLoS Pathog* 2021;**17**:e1010037. https://doi.org/10.1371/journal.ppat.1010037.

Petitpas I, Grune T, Bhattacharya AA *et al.* Crystal structures of human serum albumin complexed with monounsaturated and polyunsaturated fatty acids. *J Mol Biol* 2001;**314**:955–60. https://doi.org/10.1006/jmbi.2000.5208.

Phan QT, Myers CL, Fu Y *et al.* Als3 is a *Candida albicans* invasin that binds to cadherins and induces endocytosis by host cells. *PLoS Biol* 2007;**5**:e64. https://doi.org/10.1371/journal.pbio.0050064.

Pinsky M, Roy U, Moshe S *et al.* Human serum albumin facilitates heme-iron utilization by Fungi. *mBio* 2020;**11**. https://doi.org/10.1128/mBio.00607-20.

Psychogios N, Hau DD, Peng J *et al.* The human serum metabolome. *PLoS One* 2011;**6**:e16957. https://doi.org/10.1371/journal.pone.0016957.

Rodrigues AG, Araujo R, Pina-Vaz C. Human albumin promotes germination, hyphal growth and antifungal resistance by *Aspergillus fumigatus*. *Med Mycol* 2005;**43**:711–7. https://doi.org/10.1080/13693780500129814.

Rossoni RD, Barbosa JO, Vilela SF *et al.* Competitive interactions between *C. albicans*, *C. glabrata* and *C. krusei* during biofilm formation and development of experimental candidiasis. *PLoS One* 2015;**10**:e0131700. https://doi.org/10.1371/journal.pone.0131700.

Rossoni RD, Dos Santos Velloso M, Figueiredo LMA *et al.* Clinical strains of *Lactobacillus* reduce the filamentation of *Candida albicans* and protect *Galleria mellonella* against experimental candidiasis. *Folia Microbiol* 2018;**63**:307–14. https://doi.org/10.1007/s12223-017-0569-9.

Rueda C, Cuenca-Estrella M, Zaragoza O. Paradoxical growth of *Candida albicans* in the presence of caspofungin is associated with multiple cell wall rearrangements and decreased virulence. *Antimicrob Agents Chemother* 2014;**58**:1071–83. https://doi.org/10.1128/AAC.00946-13.

Rueden CT, Schindelin J, Hiner MC *et al.* ImageJ2: imageJ for the next generation of scientific image data. *BMC Bioinf* 2017;**18**:529. https://doi.org/10.1186/s12859-017-1934-z.

Ruhland E, Siemers M, Gerst R *et al.* The global RNA–RNA interactome of *Klebsiella pneumoniae* unveils a small RNA regulator of cell division. *Proc Natl Acad Sci USA* 2024;**121**. https://doi.org/10.1073/pnas.2317322121.

Saville SP, Lazzell AL, Monteagudo C *et al.* Engineered control of cell morphology in vivo reveals distinct roles for yeast and filamentous forms of *Candida albicans* during infection. *Euk Cell* 2003;**2**:1053–60. https://doi.org/10.1128/EC.2.5.1053-1060.2003.

Schindelin J, Rueden CT, Hiner MC *et al.* The ImageJ ecosystem: an open platform for biomedical image analysis. *Mol Reproduct Dev* 2015;**82**:518–29. https://doi.org/10.1002/mrd.22489.

Schmidt F, Thywissen A, Goldmann M *et al.* Flotillin-dependent membrane microdomains are required for functional phagolysosomes against fungal infections. *Cell Rep* 2020;**32**:108017. https://doi.org/10.1016/j.celrep.2020.108017.

Schonherr FA, Sparber F, Kirchner FR *et al.* The intraspecies diversity of *C. albicans* triggers qualitatively and temporally distinct host responses that determine the balance between commensalism and pathogenicity. *Mucosal Immunology* 2017;**10**:1335–50. https://doi.org/10.1038/mi.2017.2.

Shapiro RS, Robbins N, Cowen LE. Regulatory circuitry governing fungal development, drug resistance, and disease. *Microbiol Mol Biol Rev* 2011;**75**:213–67. https://doi.org/10.1128/MMBR.00045-10.

Siles SA, Srinivasan A, Pierce CG *et al.* High-throughput screening of a collection of known pharmacologically active small compounds for identification of *Candida albicans* biofilm inhibitors. *Antimicrob Agents Chemother* 2013;**57**:3681–7. https://doi.org/10.1128/AAC.00680-13.

Simonetti N, Strippoli V, Cassone A. Yeast-mycelial conversion induced by N-acetyl-D-glucosamine in *Candida albicans*. *Nature* 1974;**250**:344–6. https://doi.org/10.1038/250344a0.

Siscar-Lewin S, Hube B, Brunke S. Antivirulence and avirulence genes in human pathogenic fungi. *Virulence* 2019;**10**:935–47. https://doi.org/10.1080/21505594.2019.1688753.

Soille P, Vincent L. Determining watersheds in digital pictures via flooding simulations. In: *Proceedings of the Visual Communications and Image Processing '90*. Vol. **1360**. Bellingham, WA: SPIE, 1990.

Song S, Zhao S, Sun X *et al.* Anti-virulence strategy of diaryl chalcogenide compounds against *Candida albicans* infection. *Virulence* 2023;**14**:2265012. https://doi.org/10.1080/21505594.2023.2265012.

Sprague JL, Schille TB, Allert S *et al. Candida albicans* translocation through the intestinal epithelial barrier is promoted by fungal zinc acquisition and limited by NFkappaB-mediated barrier protection. *PLoS Pathog* 2024;**20**:e1012031. https://doi.org/10.1371/journal.ppat.1012031.

Staab JF, Bradway SD, Fidel PL *et al.* Adhesive and mammalian transglutaminase substrate properties of *Candida albicans* Hwp1. *Science* 1999;**283**:1535–8. https://doi.org/10.1126/science.283.5407.1535.

Staib F. Serum-proteins as nitrogen source for yeastlike fungi. *Med Mycol* 1966;**4**:187–93. https://doi.org/10.1080/00362176685190421.

Sudbery PE. The germ tubes of *Candida albicans* hyphae and pseudohyphae show different patterns of septin ring localization. *Mol Microbiol* 2001;**41**:19–31. https://doi.org/10.1046/j.1365-2958.2001.02459.x.

Sudbery PE. Growth of *Candida albicans* hyphae. *Nat Rev Microbiol* 2011;**9**:737–48. https://doi.org/10.1038/nrmicro2636.

Tams RN, Wagner AS, Jackson JW *et al.* Pathways that synthesize phosphatidylethanolamine impact *Candida albicans* hyphal length and cell wall composition through transcriptional and posttranscriptional mechanisms. *Infect Immun* 2020;**88**. https://doi.org/10.1128/IAI.00480-19.

Taschdjian CL, Burchall JJ, Kozinn PJ. Rapid identification of *Candida albicans* by filamentation on serum and serum substitutes. *Arch Pediatr Adolesc Med* 1960;**99**:212–5. https://doi.org/10.1001/archpedi.1960.02070030214011.

Taverna M, Marie AL, Mira JP *et al.* Specific antioxidant properties of human serum albumin. *Ann Intensive Care* 2013;**3**:4. https://doi.org/10.1186/2110-5820-3-4.

Taylor BN, Hannemann H, Sehnal M *et al.* Induction of SAP7 correlates with virulence in an intravenous infection model of candidiasis but not in a vaginal infection model in mice. *Infect Immun* 2005;**73**:7061–3. https://doi.org/10.1128/IAI.73.10.7061-7063.2005.

Tessler M, Dascal A, Gioseffini S *et al.* Growth curves of *Staphylococcus aureus*, *Candida albicans*, and *Moraxella osloensis* in propofol and other media. *Can J Anaesth* 1992;**39**:509–11. https://doi.org/10.1007/BF03008718.

Tucey TM, Verma J, Olivier FAB *et al.* Metabolic competition between host and pathogen dictates inflammasome responses to fungal infection. *PLoS Pathog* 2020;**16**:e1008695. https://doi.org/10.1371/journal.ppat.1008695.

Uhl MA, Biery M, Craig N *et al.* Haploinsufficiency-based large-scale forward genetic analysis of filamentous growth in the diploid human fungal pathogen *C. albicans*. *EMBO J* 2003;**22**:2668–78. https://doi.org/10.1093/emboj/cdg256.

Uwamahoro N, Verma-Gaur J, Shen HH *et al.* The pathogen *Candida albicans* hijacks pyroptosis for escape from macrophages. *mBio* 2014;**5**:e00003–14. https://doi.org/10.1128/mBio.00003-14.

van der Vusse GJ. Albumin as fatty acid transporter. *Drug Metab Pharmacokinet* 2009;**24**:300–7. https://doi.org/10.2133/dmpk.24.300.

Villa S, Hamideh M, Weinstock A *et al.* Transcriptional control of hyphal morphogenesis in *Candida albicans*. *FEMS Yeast Res* 2020;**20**. https://doi.org/10.1093/femsyr/foaa005.

Wakade RS, Huang M, Mitchell AP *et al.* Intravital imaging of *Candida albicans* identifies differential *in vitro* and *in vivo* filamentation phenotypes for transcription factor deletion mutants. *mSphere* 2021;**6**:e0043621. https://doi.org/10.1128/mSphere.00436-21.

Wakade RS, Kramara J, Wellington M *et al. Candida albicans* filamentation does not require the cAMP-PKA pathway In Vivo. *mBio* 2022;**13**:e0085122. https://doi.org/10.1128/mbio.00851-22.

Wakade RS, Ristow LC, Wellington M *et al.* Intravital imaging-based genetic screen reveals the transcriptional network governing *Candida albicans* filamentation during mammalian infection. *eLife* 2023;**12**. https://doi.org/10.7554/eLife.85114.

Wang R, Liu J, Liu Y *et al.* Application of the mutant libraries for *Candida albicans* functional genomics. *Int J Mol Sci* 2022;**23**:12307. https://doi.org/10.3390/ijms232012307.

Wartenberg A, Linde J, Martin R *et al.* Microevolution of *Candida albicans* in macrophages restores filamentation in a nonfilamentous mutant. *PLoS Genet* 2014;**10**:e1004824. https://doi.org/10.1371/journal.pgen.1004824.

Westman J, Walpole GFW, Kasper L *et al.* Lysosome fusion maintains phagosome integrity during fungal infection. *Cell Host Microbe* 2020;**28**:798–812.e6. https://doi.org/10.1016/j.chom.2020.09.004.

Wurster S, Kumaresan PR, Albert ND *et al.* Live monitoring and analysis of fungal growth, viability, and mycelial morphology using the IncuCyte NeuroTrack processing module. *mBio* 2019;**10**. https://doi.org/10.1128/mBio.00673-19.

Received 16 December 2024; **revised** 28 February 2025; **accepted** 12 March 2025